BRIDGED MICROMECHANICAL FILTERS

Sheng-Shian Li, Mustafa U. Demirci, Yu-Wei Lin, Zeying Ren, and Clark T.-C. Nguyen

Center for Wireless Integrated Micro Systems
Department of Electrical Engineering and Computer Science
University of Michigan, Ann Arbor, Michigan 48109-2122, USA

***Abstract*—High-order micromechanical filters comprised of 3 to 4 mechanically coupled resonators, and employing for the first time "bridging" between nonadjacent resonators to affect loss poles for better filter shape factors, have been demonstrated using a polysilicon surface micromachining technology with insertion loss less than 3 dB, sharper passband-to-stopband roll-offs than achievable by equivalent non-bridged filters, and around 50 dB of stopband rejection—15 dB better than a previous 2-resonator filter design. The filters of this work consist of several clamped-clamped beam resonators with a more general coupling scheme than previously used, where non-adjacent, as well as adjacent, resonators are coupled to generate loss poles, leading to frequency characteristics with faster roll-offs from passband to stopband and greater stopband rejections. Via this bridging design approach, 20 dB shape factors down to 1.95 have been achieved for filters centered at 9 MHz using only 3 resonators.**

***Keywords*—micromechanical filter, coupling, bandpass, high-order, loss pole, shape factor, stopband rejection**

I. INTRODUCTION

Vibrating mechanical tank components, such as crystal and SAW resonators, are widely used to implement bandpass filters in the radio frequency (RF) and intermediate frequency (IF) stages of heterodyning transceivers. Due to orders of magnitude higher quality factor Q, filters utilizing such technologies greatly outperform comparable filters implemented using conventional transistor technologies in insertion loss, percent bandwidth, and achievable rejection. However, being off-chip components, these mechanical devices must interface with integrated electronics at the board level, and this constitutes an important bottleneck against miniaturization and performance of super-heterodyne transceivers. For this reason, recent attempts to miniaturize transceivers for cellular applications have utilized alternative architectures (e.g., direct-conversion [1], wideband-IF [2], or direct sub-sampling [3]) that attempt to eliminate the need for high-Q IF components, but at the price of performance, and without a solution for removing the RF passives. Given that the number of RF passives is expected to increase in future multi-band wireless applications, methods for miniaturizing high-Q passives (both IF and RF), while maintaining more robust super-heterodyne architectures, are becoming increasingly attractive.

The rapid growth of micromachining technologies that yield high-Q on-chip micromechanical ("μmechanical") resonators [4][5][6] now suggests a method for miniaturizing and integrating the highly selective filters alongside transistor circuits, with the intent of perhaps someday enabling single-chip super-heterodyne transceivers. With Q's of over 150,000 under vacuum (and 10,000 in air) [7] and center frequency temperature coefficients as low as -0.24 ppm/°C [8], polycrystalline silicon μmechanical resonators can potentially serve well as miniaturized high-Q resonators in a variety of oscillator and filtering applications. To date, two-resonator (i.e., fourth-order) prototypes of such filters have been demonstrated from low frequency (LF) to very high frequency (VHF) [9][10], and three-resonator (i.e., sixth order) prototypes in the LF range [11]. For use in communications, however, sharper roll-offs and larger stopband rejections than previously achieved using micromechanics are often required, and thus, higher order filters with loss poles in their frequency characteristics are desirable.

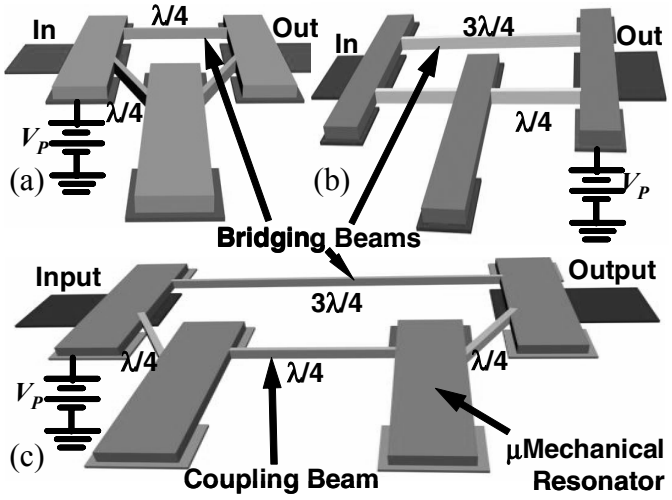

Fig. 1: Perspective-view schematics for the three bridged μmechanical filter designs realized in this work. (a) 3CC filter with λ/4 bridging beam design (3CC λ/4). (b) 3CC filter with 3λ/4 bridging beam design (3CC 3λ/4). (c) 4CC filter with 3λ/4 bridging beam design (4CC 3λ/4).

In this work, high-order μmechanical filters comprised of 3 to 4 mechanically coupled resonators, and employing for the first time (on the micro-scale) "bridging" between nonadjacent resonators [12] to affect loss poles for better filter shape factors, have been demonstrated with sharper passband-to-stopband roll-offs than achievable by equivalent non-bridged filters [9][11], and with around 50 dB of stopband rejection—15 dB better than a previous 2-resonator filter design [9]. Via this bridging design approach, depicted in Fig. 1, shape factors down to 1.95 have been achieved for filters centered at 9 MHz using only 3 resonators. This work stands to greatly reduce the number of resonators needed in a

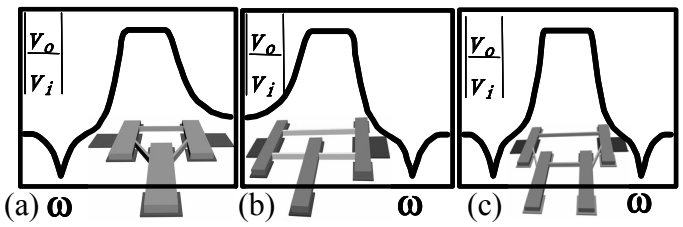

Fig. 2: Expected frequency characteristics for the bridged μmechanical filters of Fig. 1(a)-(c), respectively.

μmechanical filter to achieve a given shape factor.

II. Filter Structure and Operation

Fig. 1 presents schematics for the bridged μmechanical filter designs of this work. As shown, each of these filters consists of several clamped-clamped beam ("CC-beam") resonators coupled mechanically by soft flexural-mode beams, all suspended 1000 Å above the substrate. Conducting strips underlie the central region of each end resonator and serve as capacitive transducer electrodes positioned to induce resonator vibration in a direction perpendicular to the substrate. The resonator-to-electrode gaps are targeted for 1000 Å. Of the three different designs in Fig. 1, (a) and (b) are three resonator filters, while (c) is a four resonator filter.

Previous μmechanical filters [9][11] utilized only coupling between adjacent resonators, leading to frequency characteristics with monotonic stopbands. In contrast, the bridged filters of this work employ a more general coupling scheme, where non-adjacent resonators are now linked. As shown, non-adjacent resonator coupling is achieved by offsetting the inner resonators from the outer ones to allow direct mechanical coupling of outer resonators in the same structural layer (i.e., without the need for a third layer of polysilicon). In this coupling scheme, previously described low velocity coupling strategies [9] to set the overall filter bandwidth are still available and are utilized to advantage in this work. As depicted in Fig. 1, some of the filter variants use angled adjacent-resonator coupling beams in order to minimize the length of the non-adjacent resonator coupler. For example, by using angled adjacent-resonator couplers, the design of (a) can use a quarter-wavelength (λ/4) non-adjacent resonator coupler, whereas the straight adjacent-resonator coupler design of (b) must use three-quarter-wavelength (3λ/4) couplers. Even with an angled coupler, the 4-resonator filter design of (c) still requires a 3λ/4 non-adjacent resonator coupling beam. (The need for quarter-wavelength couplers is further described in [9] and in Section III.)

In each filter structure, the new non-adjacent resonator linkage introduces a feedforward path that generates loss poles in the filter transfer function, leading to a faster roll-off from passband to stopband, as shown in Fig. 2, which plots the expected frequency characteristics corresponding to the different filter structures of Fig. 1. Here, loss poles are seen to occur either below or above the passband of a 3 CC-beam bridged filter design, depending upon whether its coupling beam dimensions correspond to a quarter-wavelength or to three-quarter-wavelengths, respectively. The 4 CC-beam

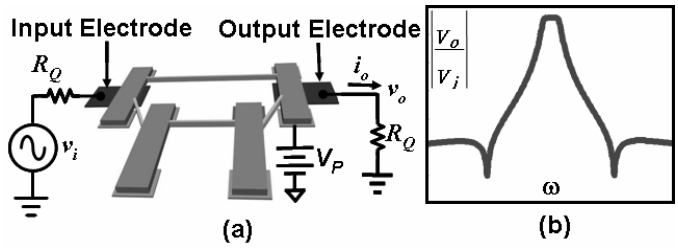

Fig. 3: (a) Perspective view schematic of a 4 CC-beam bridged filter, along with the preferred bias, excitation, and sensing circuitry. (b) Expected frequency characteristic.

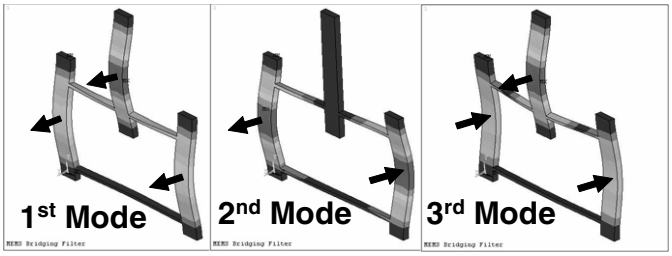

Fig. 4: Finite element simulated mode shapes for the 3CC 3λ/4 bridged μmechanical filter of Fig. 1(b).

bridged filter design, on the other hand, achieves two loss poles on each side of its passband with a symmetrical frequency response. In all cases, the loss poles provide sharper passband-to-stopband roll-offs and greater stopband rejection in their respective filter transfer functions.

To operate any one of the filters in Fig. 1, a dc-bias V_P is applied to the suspended filter structure, and an ac input voltage v_i is applied through a properly-valued input termination resistor R_Q to the input electrode, as shown in Fig. 3. This combined input generates an electrostatic force between the input electrode and the conductive resonator that induces vibration of the input resonator when the frequency of v_i is within the passband of the mechanical filter. This vibrational energy is imparted to the center and output resonators via the coupling springs, causing them to vibrate as well. Vibration of the output resonator creates a dc-biased, time varying capacitor between the conductive resonator and output electrode, which sources a motional output current i_o. The motional current is then directed to the output termination resistor R_Q, which converts the current to an output voltage and loads the Q of the output resonator so as to flatten the jagged passband (to be described via Fig. 7) of the mechanical system into the desired flat passband (to be described via Fig. 9). In effect, this device takes an electrical input signal, converts it to a mechanical signal, processes it in the mechanical domain, then reconverts the resulting signal to an electrical output signal, ready for further processing by subsequent electronic stages.

III. Bridged Filter Design and Modeling

Due to the good matching tolerance, but poor absolute tolerance, of the planar fabrication technology used to construct the subject μmechanical filters, it is advantageous to design filters so that their constituent resonators have identical uncoupled frequencies, and then just let the coupling beams pull

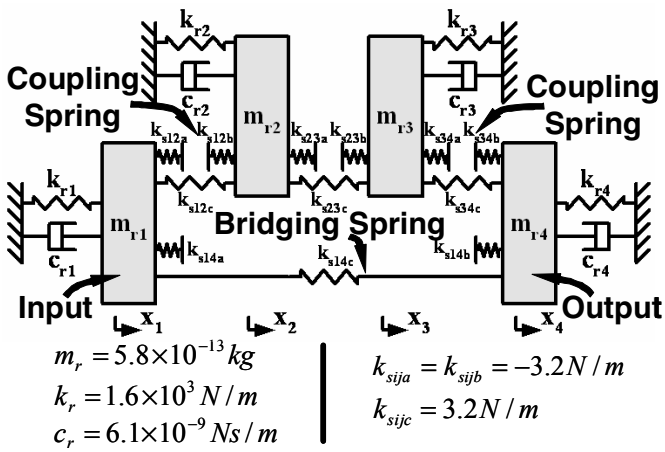

Fig. 5: Equivalent lumped mechanical model for a bridged 4 CC-beam μmechanical filter. Here, each λ/4 or 3λ/4 coupling spring is represented by a set of three springs: one positive adjoining spring, and two negative grounded springs, so as to simulate the canceling effect of quarter-wavelength design.

their frequencies apart to generate a passband [9]. In such a design, the center frequency of the filter is determined primarily by the (identical) frequencies of its constituent resonators, while the spacing between modes (i.e. the bandwidth) is determined largely by the stiffness of its coupling springs. Fig. 4 presents finite element simulations depicting the mode shapes corresponding to each of the three mode frequencies of the filter in Fig. 1(b). For the coupled three-resonator system of Fig. 1(b), the frequency of each vibration mode corresponds to a distinct peak in the force-to-displacement frequency characteristic and to a distinct, physical mode shape of the coupled mechanical system as shown in Fig. 4. In the lowest frequency mode, all resonators vibrate in phase; in the middle frequency mode, the center resonator ideally remains motionless, while the end resonators vibrate 180° out of phase; and finally, in the highest frequency mode, each resonator is phase-shifted 180° from its adjacent neighbor. Without proper impedance matching, the complete mechanical filter exhibits the jagged passband seen in the mechanical simulations of Fig. 7. As will be shown, proper impedance matching in the form of termination resistors designed to lower the *Q*'s of the input and output resonators by specific amounts are required to flatten the passband and achieve a more recognizable filter characteristic, such as in Fig. 2.

For mass balance reasons, a design with identical resonators is best achieved using coupling beams with dimensions that correspond to single- or multiple-quarter-wavelengths at the filter center frequency. Thus, as mentioned earlier, each of the three bridged filter designs implemented here, and shown in Fig. 1, utilize quarter-wavelength (λ/4) couplers between adjacent resonators, and either λ/4 or 3λ/4 (for longer distances) coupling beams to connect non-adjacent resonators. The design variations include

a) A 3 CC-beam filter using a λ/4 bridging beam (3CC λ/4) with a loss pole below the passband as shown in Fig. 2(a).

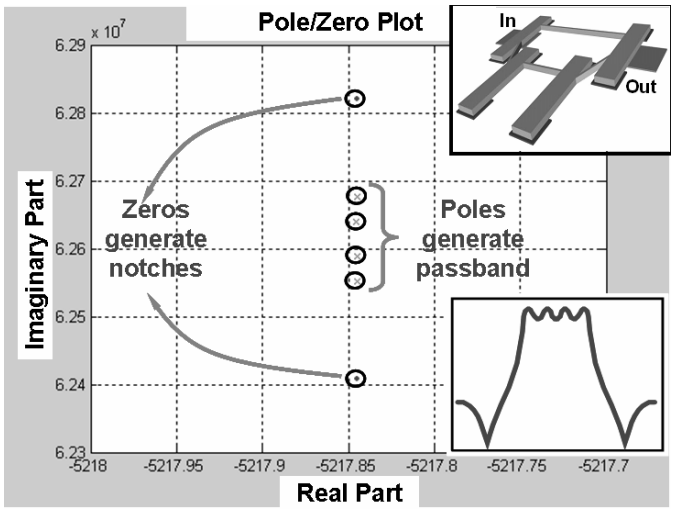

Fig. 6: Pole/zero, i.e. root locus, plot of a transfer function derived from the mechanical vibration model of the output resonator in a 4 CC-beam bridged μmechanical filter.

b) A 3 CC-beam filter using a 3λ/4 bridging beam (3CC 3λ/4) with a loss pole above the passband as shown in Fig. 2(b).

c) A 4 CC-beam filter using a 3λ/4 bridging beam (4CC 3λ/4) with two loss poles as shown in Fig. 2(c).

As mentioned in Section II, to accommodate differences in coupling beam path lengths in designs (a) and (c), angled beams are utilized to preserve λ/4 adjacent-resonator coupling.

Simple mechanical models for the filters of Fig. 1 can be attained by first recognizing that each is merely a multi-degree of freedom mechanical system that can be equated in narrow frequency bands to a lumped parameter mechanical circuit. For example, the actual filter structure of Fig. 1(c) can be explicitly equated to the equivalent mechanical circuit shown in Fig. 5, where each resonator is represented by a mass-spring-damper system, while each coupling beam, including the bridging beam, corresponds to a network of mechanical springs. The bridging beam connecting the input and output resonators provides a feedforward path that generates the desired loss poles.

Mathematically, the lumped parameter mechanical circuit of Fig. 5 (and those of the other designs in Fig. 1) can be modeled by matrix equations of the form

$$[M]\ddot{\vec{x}} + [C]\dot{\vec{x}} + [K]\vec{x} = \vec{F} \qquad (1)$$

where [*M*], [*C*], and [*K*] are the mass, damping, and stiffness matrices, respectively, and *F* is the electrostatic force applied to the input end resonator, as described in the previous section. Fig. 6 presents the computer-simulated pole/zero plot for the input-to-output resonator transfer function for the system depicted in Fig. 5 and modeled by (1), along with the actual transfer function plot. Here, the poles correspond to the mode frequencies that combine to form the passband of this bridged filter, while the zeros generate the notch profiles in its frequency response. The mechanical passband response is jagged

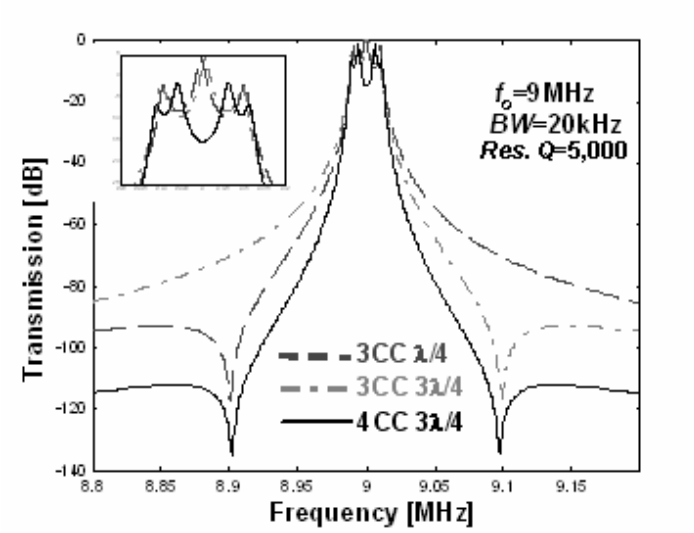

Fig. 7: Simulated frequency response spectra for the equivalent lumped mechanical models for each of the filters of Fig. 1.

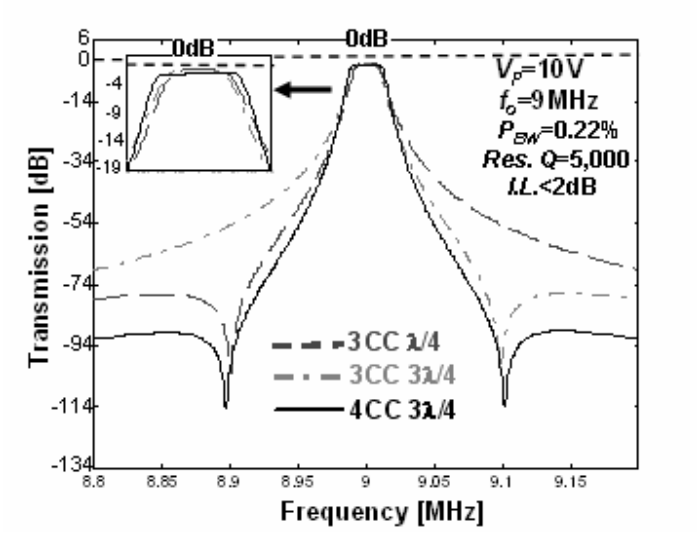

Fig. 9: SPICE-simulated frequency characteristics for the bridged 3CC λ/4, 3CC 3λ/4, and 4CC 3λ/4 μmechanical filters of Fig. 1, all properly terminated, and using electrical equivalent circuits based on the topology of Fig. 8.

at this point, but will be flattened out later (i.e., in the next section) into an eventual filter passband by properly terminating the input and output resonators. The number of mechanical resonance modes with closely spaced frequencies is equal to the number of resonators used in the filter. For example, the 3CC 3λ/4 design simulated via ANSYS in Fig. 4 exhibits three mechanical resonance modes.

Fig. 7 presents simulated frequency characteristics for each of the bridged filter designs explored in this work using their lumped parameter mechanical models. As shown, the loss pole for the 3CC λ/4 design occurs below the passband, while that for the 3CC 3λ/4 design is generated above the passband. And as expected from Fig. 2(c), the 4CC 3λ/4 design exhibits two loss poles around a symmetrical frequency response. Among the three design variations, the 4CC 3λ/4 design demonstrates the best filter shape factor and largest stopband rejection, albeit via the use of more mechanical links and resonators.

IV. ELECTRICAL EQUIVALENT CIRCUIT

Although the described mechanical circuit model is helpful in gaining an analytical understanding of bridged filter operation, an electrical equivalent circuit model would be more useful for design verification and evaluation in actual communication systems, since it would allow the use of the abundant and well-developed electrical circuit simulators in existence, such as SPICE [13]. The electrical equivalent circuit can be derived by mere analogy to the mechanical circuit of Section III, where each mass is replaced by an inductor, each spring by a capacitor, and each damper by a resistor.

Taking this approach, Fig. 8 presents the electrical equivalent circuit with element values for the 4CC 3λ/4 design (depicted in Fig. 1(c)), for which the mechanical circuit has already been given in Fig. 5. As shown, each resonator origi-

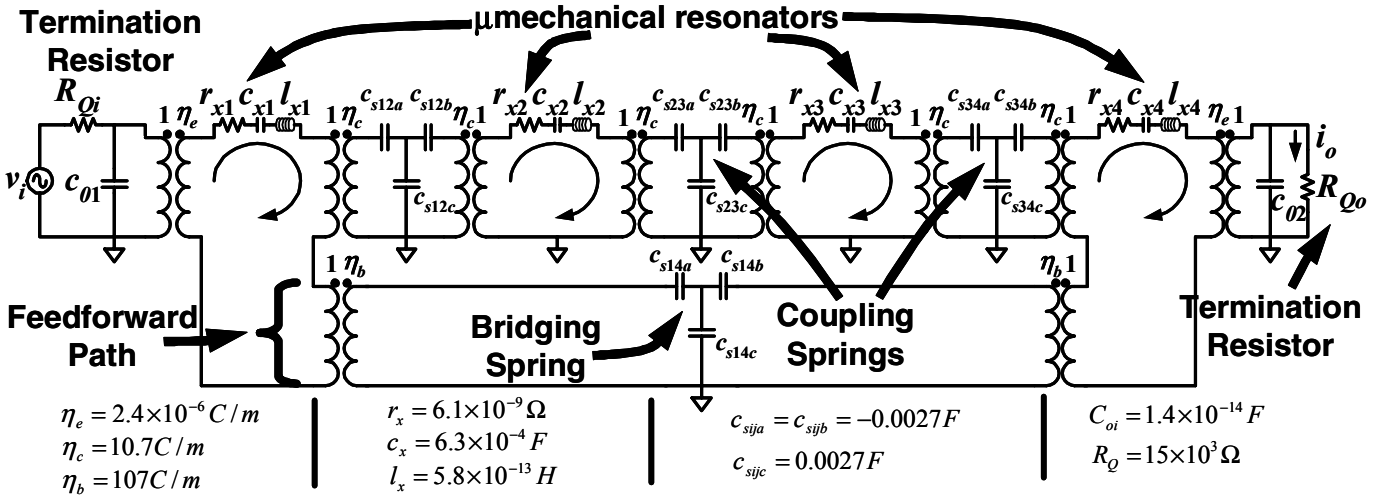

Fig. 8: Equivalent electrical circuit for a 4 CC-beam μmechanical filter using a three-quarter-wavelength (3λ/4) bridging beam.

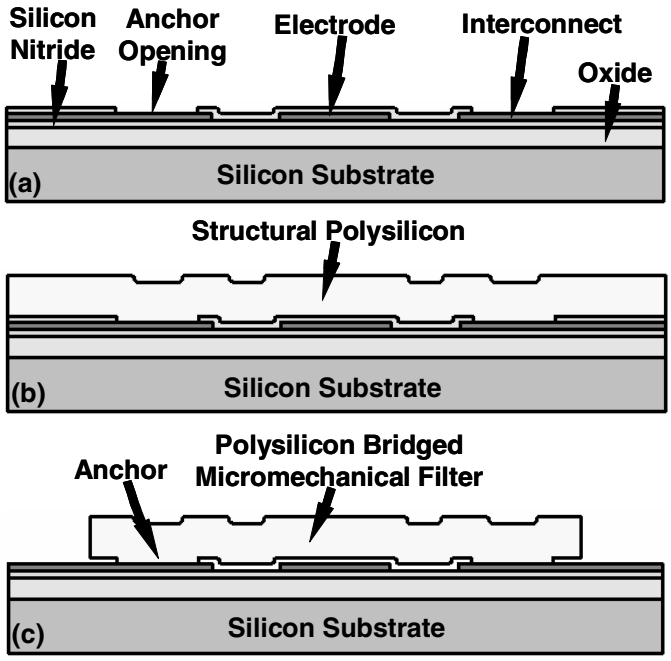

Fig. 10: Cross-sections depicting the fabrication sequence used to achieve the bridged μmechanical filters. (a) polysilicon electrode and interconnect layers under a 1000-Å-thick sacrificial oxide, (b) 2-μm-thick structural polysilicon layer, and (c) resulting free-standing beam following a release etch in hydrofluoric acid.

nally represented by a mass-spring-damper is now modeled by an *LCR* circuit. The coupling beams are actually mechanical transmission lines, so are equated to *T* networks of energy storage elements—usually a combination of capacitors and inductors, but in this case, a combination of positive and negative valued capacitors (where the negative valued ones are essentially inductors) to emphasize the quarter-wavelength canceling nature of the coupling beams [9]. Note that Fig. 8 clearly shows the bridging connection as a feedforward path in the electrical domain.

Fig. 9 presents spice simulations (using equivalent circuits similar to that of Fig. 8 with appropriately valued [9] termination resistors R_{Qi}=R_{Qo}=15 kΩ) comparing the expected frequency characteristics for each of the three designs. As shown, the 3CC design has one loss pole, which occurs below the passband when a λ/4 bridging beam is used, and above when a 3λ/4 is used. The 4CC design achieves two loss poles with a 3λ/4 bridging beam. As advertised, the frequency responses are similar to those of the mechanical simulations of Fig. 7, except these show flat passbands and the actual (small) filter insertion loss, since they are properly terminated with R_{Qi} and R_{Qo}. Like the response in mechanical domain, the 4CC 3λ/4 design exhibits the best filter shape factor among the three, although it has slightly larger insertion loss in the electrical domain.

V. Fabrication and Experimental Results

Bridged μmechanical filters were fabricated using a previously described small-vertical gap surface-micromachining technology [9], summarized by the process cross-sections of Fig. 10. In this process, a 2-μm-thick silicon dioxide and 3500-Å-thick silicon nitride are first deposited on the silicon substrate to serve as a top layer that electrically isolates me-

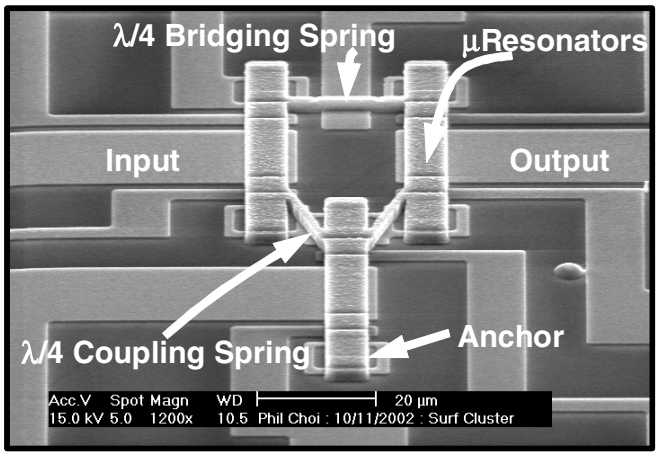

Fig. 11: Scanning electron micrograph (SEM) of a 3CC λ/4 bridged μmechanical filter.

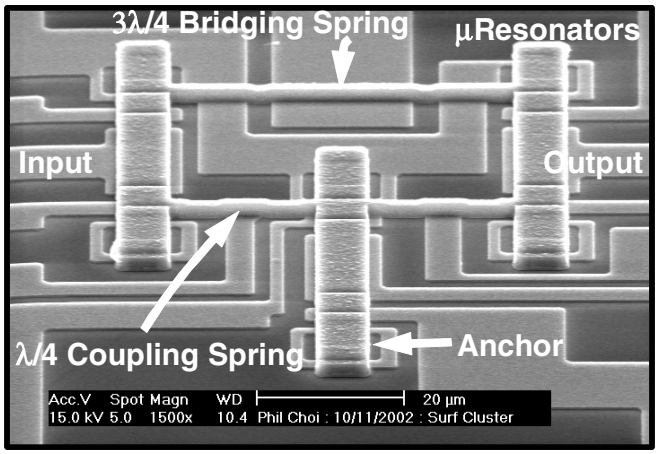

Fig. 12: Scanning electron micrograph (SEM) of a 3CC 3λ/4 bridged μmechanical filter.

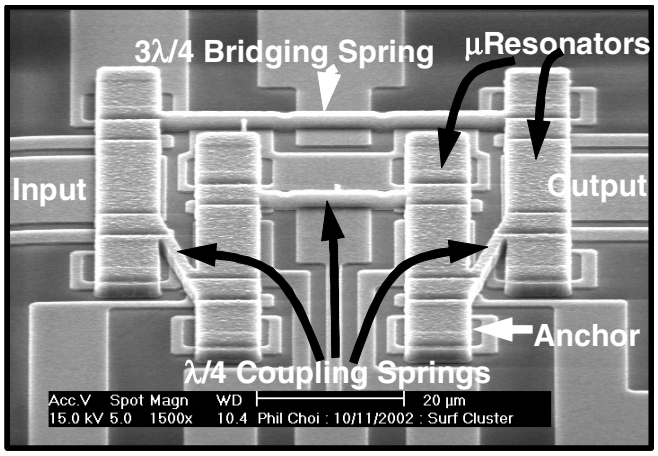

Fig. 13: Scanning electron micrograph (SEM) of a 4CC 3λ/4 bridged μmechanical filter.

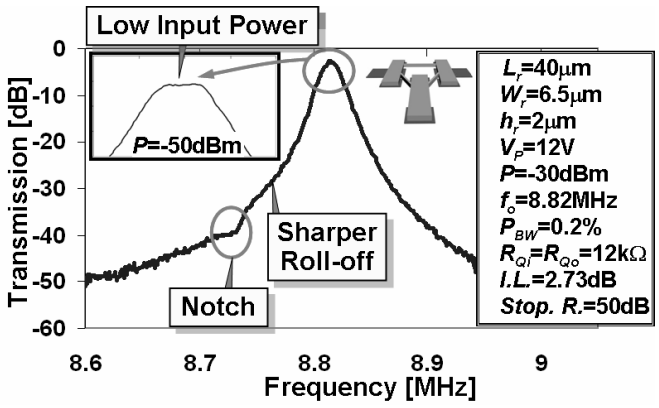

Fig. 14: Measured frequency characteristic for 3CC λ/4 bridged micromechanical filter of Fig. 11. The flat passband shown in the upper left corner is obtained with a lower input power level.

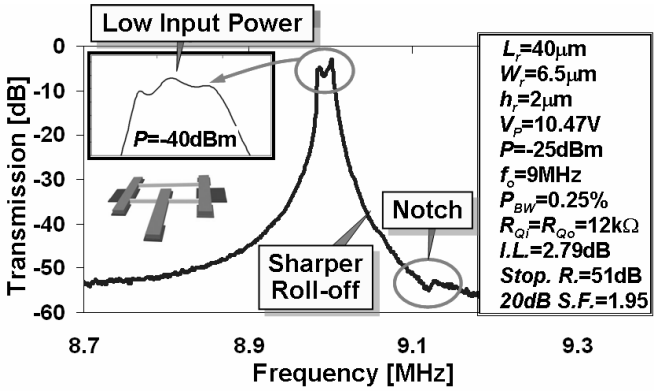

Fig. 15: Measured frequency characteristic for 3CC 3λ/4 bridged μmechanical filter of Fig. 12. The rippled passband (three humps) shown in the upper left corner is obtained with a lower input power level.

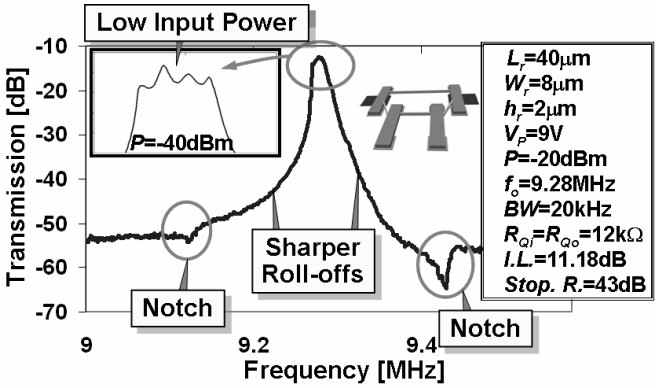

Fig. 16: Measured frequency characteristic for the 4CC 3λ/4 bridged μmechanical filter of Fig. 13. The rippled passband (four humps) shown in the upper left corner is obtained with a lower input power level.

chanical devices and interconnects from the substrate and from themselves. A 3000-Å-thick polysilicon layer is then deposited, doped, and patterned, to serve as input/output electrodes and electrical interconnect. Next, a 1000-Å-thick sacrificial silicon dioxide layer is deposited to define the gap spacing between resonators and electrodes. An RIE etch then defines anchors, as shown in Fig. 10(a), and a 2-μm-thick polysilicon layer is deposited, doped, and patterned, to define the beam structure shown in Fig. 10(b). Finally, hydrofluoric acid is used to remove the sacrificial oxide and release the structural layer, leaving a free-standing structure shown in Fig. 10(c). Fig. 11-Fig. 13 present SEM's for fabricated versions of each design.

Fig. 14-Fig. 16 present frequency characteristics for each design, measured under 200 μTorr vacuum using a custom-built vacuum chamber together with a network analyzer, and using the indicated bias configurations of Fig. 3 with 12 kΩ input and output termination resistors. As shown in Fig. 14, the 3CC λ/4 design achieves an insertion loss of only 2.73 dB for a 0.2% bandwidth centered at 8.82 MHz, with 50 dB of stopband rejection, and a (notch) loss pole below the passband, as expected. For input powers lower than -50 dBm, a flat passband could be obtained as shown in the top left of Fig. 14, but the notch profile below the passband becomes masked by the noise floor. From Fig. 15, the 3CC 3λ/4 design achieves an insertion loss of 2.79 dB for a 0.25% bandwidth centered at 9 MHz, with 51 dB of stopband rejection, a loss pole above the passband, and a shape factor of only 1.95—much better than achieved in [9]. Again, for low input power levels, a passband with the designed ripple is seen, shown in the top left of Fig. 15, but the notch profile above the passband becomes masked by the measurement noise floor. From Fig. 16, the 4CC 3λ/4 design achieves comparable characteristics, but with two loss poles, hence, even better shape factor in theory. (Duffing nonlinearity in the filter transfer function prevents exact determination of the shape factor from Fig. 16.). Like the other filters, the designed rippled passband of the 4CC 3λ/4 design can be seen at lower input power levels.

VI. CONCLUSIONS

High-order μmechanical filters employing for the first time "bridging" between nonadjacent resonators to affect loss poles have been designed and demonstrated in an IC-compatible polysilicon surface-micromachining technology. These bridged filters utilize fewer resonators to achieve sharper passband-to-stopband roll-offs, larger stopband rejections, and smaller filter shape factors, than previous non-bridged micromechanical filters. In particular, compared with previous 2-resonator designs, the 3 CC-beam filters using either λ/4 or 3λ/4 coupling bridges achieve very low insertion loss with more than 50 dB of stopband rejection, and 20 dB shape factors down to 1.95 at 9 MHz. With the above successes, the bridging filter design techniques explored here are expected to greatly benefit future communication systems, especially when transferred to UHF frequencies using newer disk-type resonators [14] that can handle more power, hence avoid Duffing nonlinearities. These bridging design strategies will likely become increasingly important as frequency and filter performance requirements rise to accommodate the needs of future multi-band wireless transceivers.

Acknowledgment. This work was supported by DARPA and an NSF ERC on Wireless Integrated Microsystems.

References.

[1] A. A. Abidi, “Direct-conversion radio transceivers for digital communications,” *IEEE J. Solid-State Circuits*, vol. 30, No. 12, pp. 1399-1410, Dec. 1995.

[2] J. C. Rudell, J.-J. Ou, T. B. Cho, G. Chien, F. Brianti, J. A. Weldon, and P. R. Gray, “A 1.9-GHz wide-band IF double conversion CMOS receiver for cordless telephone applications,” *IEEE J. Solid-State Circuits*, vol. 32, no. 12, pp. 2071-2088, Dec. 1997.

[3] D. Shen, C. M. Hwang, B. Lusignan, B. A. Wooley, “A 900 MHz RF front-end with integrated discrete-time filtering,” *IEEE J. Solid-State Circuits*, vol. 31, no. 12, pp. 1945-1954, Dec. 1996.

[4] S.-S. Li, Y.-W. Lin, Y. Xie, Z. Ren, and C. T.-C. Nguyen, “Micromechanical “hollow-disk” ring resonators,” *Technical Digest*, IEEE Int. Conf. on Micro Electro Mechanical Systems, Maastricht, The Netherlands, 2004, pp. 821-824.

[5] J. Wang, J. Butler, T. Feygelson, and C. T.-C. Nguyen, ”1.51-GHz nanocrystalline diamond micromechanical disk resonator with material-mismatched isolating support,” *Technical Digest*, IEEE Int. Conf. on Micro Electro Mechanical Systems, Maastricht, The Netherlands, 2004, pp. 641-644.

[6] L. Yan, W. Pang, J. Wu, W. C. Tang, and E.-S. Kim, “High frequency micromechanical piezo actuated disk resonator,” *Technical Digest*, Solid-State Sensor, Actuator and Microsystems Workshop (Hilton-Head’04), Hilton Head Island, South Carolina, June 6-10, 2004, pp.372-375.

[7] Y.-W. Lin, S. Lee, S.-S. Li, Y. Xie, Z. Ren, and C. T.-C. Nguyen, ”Series-resonant VHF micromechanical resonator reference oscillators” to be published by J. Solid-State Circuits.

[8] W.-T. Hsu and C. T.-C. Nguyen, “Stiffness-compensated temperature-insensitive micromechanical resonators,” *Technical Digest*, IEEE Int. Conf. on Micro Electro Mechanical Systems, Las Vegas, NV, 2002, pp. 731-734.

[9] F. D. Bannon, J. R. Clark, and C. T.-C. Nguyen, “High-*Q* HF micromechanical filters,” *IEEE J. Solid-State Circuits*, vol. 35, no. 4, pp. 512-526, April 2000.

[10] A.-C. Wong, J. R. Clark, and C. T.-C. Nguyen, “Anneal-activated, tunable, 65MHz micromechanical filters,” *Digest of Technical Papers*, 10th International Conference on Solid-State Sensors and Actuators, Sendai, Japan, June 7-10, 1999, pp. 1390-1393.

[11] K. Wang and C. T.-C. Nguyen, “High-order medium frequency micromechanical electronic filters,” *IEEE/ASME J. Microelectromechanical Systems*., vol. 8, no. 4, pp. 534-557, 1999.

[12] R. A. Johnson, *Mechanical Filters in Electronics*. New York, NY: Wiley, 1983.

[13] Star-Hspice Manual, Release 1998.2, July 1998.

[14] J. R. Clark, W. T. Hsu, and C. T.-C. Nguyen, “High-*Q* VHF micromechanical contour-mode disk resonators,” *Technical Digest, IEEE Int. Electron Devices Meeting*, San Francisco, California, Dec. 11-13, 2000, pp. 399-402.